

A blue repulsive potential for dysprosium Bose-Einstein condensates

Niccolò Preti,^{1,2,3,*} Nicolò Antolini,^{1,2,3} Giulio Biagioni,^{1,2,3} Andrea Fioretti,³ Giovanni Modugno,^{1,2,3} Luca Tanzi,^{3,2} and Carlo Gabbanini^{3,†}

¹*Dipartimento di Fisica e Astronomia, Università di Firenze*

²*European Laboratory for Nonlinear Spectroscopy (LENS), Università di Firenze*

³*Consiglio Nazionale delle Ricerche - Istituto Nazionale di Ottica, sede secondaria di Pisa*
(Dated: March 28, 2024)

Short-wavelength repulsive potentials for quantum gases allow to realize new systems and to study new phenomena. Here we report the realization of repulsive optical potentials for dysprosium atoms in the blue region of the spectrum, at wavelengths close to 400 nm. We employ a spectrally-filtered diode laser system to measure both scalar and tensorial components of the polarizability of dysprosium, which we find in good agreement with the theoretical predictions. We demonstrate the implementation of potential strengths appropriate to manipulate Bose-Einstein condensates, with scattering-limited lifetimes exceeding one second. This type of optical potentials opens interesting directions for the study of dipolar superfluids and supersolids.

I. INTRODUCTION

Short-wavelength, repulsive optical potentials are key tools to study fundamental phenomena in ultracold quantum gases. Notable examples are uniform Bose [1] and Fermi gases [2], device-like systems [3], controllable disorder [4], and controllable vortexes [5]. Repulsive potentials are favored over attractive ones by the fact that the atoms reside mostly in the dark, limiting negative effects such as inelastic light scattering or unwanted disorder due to optical fringes. Since the minimum length scale of an optical potential is set by the related wavelength, through diffraction, to achieve the highest spatial resolution it is necessary to employ light towards the blue region of the visible spectrum.

Strongly dipolar lanthanide atoms like dysprosium or erbium are opening new directions of study in the context of quantum gases, because the presence of the long-ranged dipolar interaction leads to novel phenomena and phases, such as quantum droplets [6], supersolids [7–9] and dipolar solids [10]. So far, the realization of optical potentials for lanthanides has however been limited to the near-infrared or mid-visible regions of the spectrum [11–14], despite the fact that atomic species possess strong absorption lines in the blue region. One of the complexities of lanthanides is the relevance of all three components of the polarizability, scalar, vectorial and tensorial, which makes both the theoretical analysis and the experimental control of the optical polarizability more difficult than for other atomic species [15, 16].

In this work we study the realization of repulsive potentials for dysprosium at wavelengths close to the group of strong lines from 405 nm to 421 nm. We investigate experimentally the region between 403 and 404 nm, developing a tunable laser system based on commercially available diode lasers, spectrally filtered to avoid near-

resonant components of the background emission. Studying the mechanical effect of light on a dysprosium Bose-Einstein condensate in a combined infrared-blue potential, we measure both scalar and tensorial components of the polarization, finding a good agreement with the theory. We demonstrate that with few mW of light it is possible to obtain potential depths of the order of hundreds of nK , with lifetimes of the order of one second. This opens the possibility of realizing interesting potential configurations for dipolar superfluids and supersolids such as, for example, the same ring-like geometry that was proposed long time ago by A. J. Leggett to test the differences between superfluids and supersolids [17]. Our findings, in combination with the theory, give guidance for realizing optical potentials for dysprosium in a larger region of the blue spectrum, from 400 to 425 nm.

II. THEORY

1. Atomic polarizability

When an atom interacts with a non-resonant laser field described by a polarization vector \mathbf{e} and angular frequency ω , the AC Stark shift of the atomic ground state produces an effective atom-light potential that can be modeled as [18]:

$$U(\mathbf{r}, \omega) = -\frac{\text{Re}[\alpha(\omega)]}{2\epsilon_0 c} I(\mathbf{r}). \quad (1)$$

Here ϵ_0 represents the vacuum permittivity, c the speed of light in vacuum, $I(\mathbf{r}) = \epsilon_0 c |E(\mathbf{r})|^2 / 2$ the light intensity and $\alpha(\omega)$ is a quantity characterizing the strength of the atom-light interaction called dynamical polarizability. Generally speaking, the dynamical polarizability can be decomposed into scalar, vectorial and tensorial contributions. In lanthanides like dysprosium and erbium, because of their open f shell structure, all three components of the polarizability are in general relevant and so the theoretical investigation of the atomic polar-

* niccolo.preti@unifi.it

† carlo.gabbanini@ino.cnr.it

izability is more challenging than in other atomic species [15, 16]. It is therefore important to achieve an experimental confirmation of the theory predictions [11, 13, 19]. When considering a linearly polarized laser field the vectorial contribution, being proportional to $|\mathbf{e} \times \mathbf{e}^*|$, vanishes and the quantity $\alpha(\omega)$ can be written for a state with non-zero angular momentum [20]:

$$\alpha(\omega) = \alpha_s(\omega) + \frac{3M_J^2 - J(J+1)}{J(2J-1)} \frac{3\cos^2\theta - 1}{2} \alpha_t(\omega). \quad (2)$$

Here J represents the total electronic angular momentum of the atomic ground state and M_J is the projection of J along the quantization axis, while $\alpha_s(\omega)$ and $\alpha_t(\omega)$ are the scalar and tensorial part of the dynamical polarizability, respectively. In this expression, the tensorial contribution to the total polarizability has a dependence on the angle θ between the quantization axis and the laser electric field polarization. In our case the Dy condensate is spin polarized in its Zeeman ground state through the application of a magnetic field along z . Therefore we have that $|M_J| = J = 8$ and Eq. 2 can be written in the simplified form:

$$\alpha(\omega) = \alpha_s(\omega) + \frac{3\cos^2\theta - 1}{2} \alpha_t(\omega). \quad (3)$$

Both $\alpha_s(\omega)$ and $\alpha_t(\omega)$ depend on the frequency of the laser field and on the ground state angular momentum J . Their full theoretical expressions are given by:

$$\begin{aligned} \alpha_s(\omega) &= -\frac{1}{\sqrt{3(2J+1)}} \mathcal{F}_J^{(0)}(\omega) \\ \alpha_t(\omega) &= \frac{2\sqrt{5}J(2J-1)}{\sqrt{6(2J+3)(J+1)(2J+1)}} \mathcal{F}_J^{(2)}(\omega) \end{aligned} \quad (4)$$

where we have defined

$$\begin{aligned} \mathcal{F}_J^{(k)}(\omega) &= \sum_{\beta'J'} (-1)^{J+J'} \left\{ \begin{matrix} 1 & 1 & k \\ J & J & J' \end{matrix} \right\} |\langle \beta J || \mathbf{d} || \beta' J' \rangle|^2 \times \\ &\frac{1}{\hbar} \left[\frac{1}{\omega_{\beta'J'} - \omega + i\gamma_{\beta'J'}/2} + \frac{(-1)^k}{\omega_{\beta'J'} + \omega + i\gamma_{\beta'J'}/2} \right]. \end{aligned} \quad (5)$$

In this expression, the curly brackets represent a Wigner $6-j$ symbol, and $\langle \beta J || \mathbf{d} || \beta' J' \rangle$ is the reduced dipole matrix element evaluated between the atomic ground state $|\beta J\rangle$ and a generic excited state $|\beta' J'\rangle$ characterized by an energy $\hbar\omega_{\beta'J'}$ and natural linewidth $\gamma_{\beta'J'}$. The sum in Eq. 5 is taken over all dipole-allowed transitions.

In this paper we have experimentally investigated the region close to the $4f^{10}6s^2(^5I_8) \rightarrow 4f^{10}(^5I_8)6s6p(^1P_1)(8,1)_7$ resonance around 405 nm. Because of this, in the sum defined in Eq. 5 this transition will give the most important contribution. From Eq. 4, notice that one (two)-electron atoms, having $J = 1/2$ ($J = 0$) in their ground state, have no tensorial contribution to their ground state polarizability.

2. Polarizability of Dy in the 400-nm region

For our repulsive potential we decided to use light on the blue side of the 404.7 nm line of dysprosium, which is the transition from the ground state $4f^{10}6s^2(^5I_8)$ to the excited state $4f^{10}(^5I_8)6s6p(^1P_1)(8,1)_7$, see Fig. 1 or Table I for reference. It is a strong transition, having a linewidth γ around $2\pi \times 30$ MHz [21]. We chose this region because laser diodes with output power of the order of 100 mW around 405 nm are commercially available.

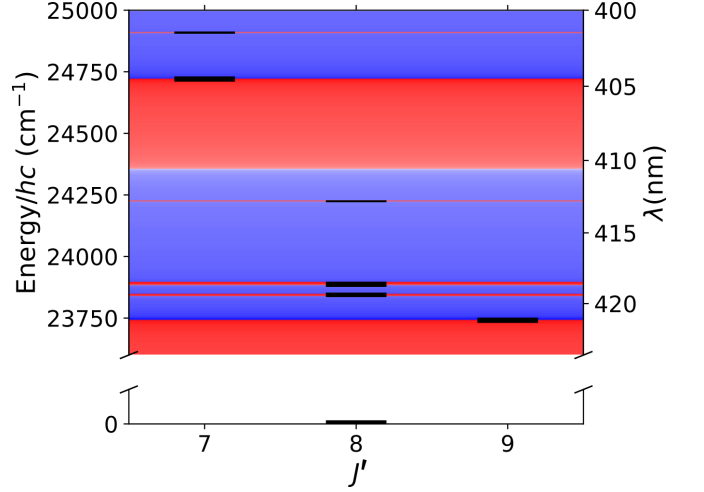


FIG. 1. Level scheme of Dy in the region of interest. Thicker black lines correspond to levels with larger linewidth. The background color scheme indicates the theoretical value of $\text{Re}[\alpha_s - \alpha_t/2]$, which is the value of the total polarizability shown in Eq. 3 for $\theta = \pi/2$. In the figure, blue (red) regions represent an overall repulsive (attractive) character.

level	J'	λ (nm)	$\gamma/2\pi$ (MHz)
$4f^{10}6s^2(^5I_8)$	8	–	–
$4f^{10}(^5I_8)6s6p(^1P_1)(8,1)_9$	9	421.3	33.1
$4f^9(^6H^0)5d^2(^3F)(^8K^0)6s$	8	419.6	14.0
$4f^{10}(^5I_8)6s6p(^1P_1)(8,1)_8$	8	418.8	20.1
$4f^9(^6H^0)5d^2(^3F)(^8I^0)6s$	8	413.2	0.3
$4f^{10}(^5I_8)6s6p(^1P_1)(8,1)_7$	7	404.7	30.6
$4f^{10}(^5I_8)6s6p(^3P_2)(6,2)_7$	7	401.5	0.5

TABLE I. Energy levels of dysprosium in the region of interest [21, 22]. Vacuum transition wavelengths from the ground state and linewidths are approximated at the first decimal position.

In Figure 2 we show the calculations of the scalar and tensorial parts of the polarizability in a range of wavelengths in the blue side of the spectrum. This plots are made using Eq. 4, where the values for $\omega_{\beta'J'}$ and $\gamma_{\beta'J'}$ of the various transitions were taken from the NIST database [21, 22]. In calculating $\mathcal{F}_J^{(k)}$, it is useful to con-

vert the reduced dipole matrix elements into linewidths using the formula:

$$|\langle \beta J \| \mathbf{d} \| \beta' J' \rangle|^2 = (2J' + 1) \frac{3\pi\epsilon_0 \hbar c^3}{\omega_{\beta' J'}^3} \gamma_{\beta' J'} \quad (6)$$

Looking at Fig. 2, we observe that the best suited spectral regions where to realize repulsive potentials are two, the first one in the approximate range (402-404) nm, and the second one in the range (415-418) nm. Both regions benefit from being on the blue side of a strong absorption line, but they differ in the sign of α_t . From 402 to 404 nm, which is the region explored experimentally in this work, α_t is positive, meaning that the maximally repulsive polarizability is achieved setting $\theta = \pi/2$ in Eq. 3, and is given by $\alpha_s - \alpha_t/2$. This region is then best suited to realize an optical potential propagating along the quantization axis, since in this case θ is geometrically fixed at $\pi/2$. In the second region, α_s and α_t share the same sign. This means that the maximally repulsive polarizability is now given by $\alpha_s + \alpha_t$, obtained putting $\theta = 0$ in Eq. 3. This makes this region the optimal one to realize a repulsive potential with light that has a polarization pointing along the quantization axis, i.e. propagating perpendicular to the quantization axis.

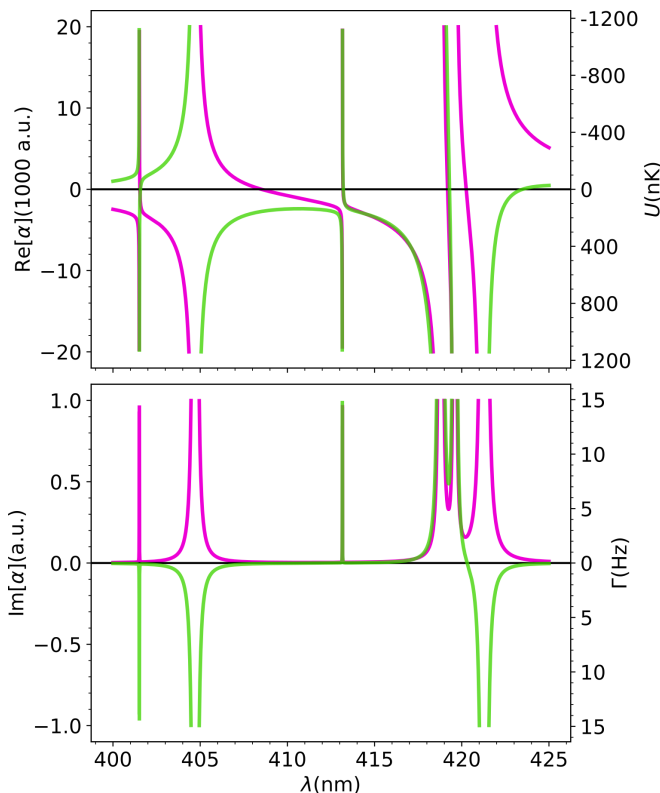


FIG. 2. Theoretical polarizability of dysprosium in the blue region. Real and imaginary part of the scalar polarizability (purple) and tensorial polarizability (green). The potential strength U and scattering rate Γ are calculated considering a laser power of 1 mW on a Gaussian beam with a waist of 50 μm .

III. EXPERIMENTAL SETUP

1. Spectrally-filtered diode laser

The light source used in the experiment is a Nichia NDV4313 diode laser with a maximum output power of 120 mW near 405 nm. Its spectrum, in free running conditions, is more than 1 nm wide, so not suitable for our scope. We therefore mounted the diode in an external cavity with Littrow configuration, using a holographic grating with 3600 grooves/mm. In this configuration, the laser becomes single-mode up to an output power of about 20 mW, with a tunability of about 1 nm changing the grating angle. We monitor the laser spectrum with a scanning Fabry-Perot interferometer (Thorlabs SA200-3B), and we measure the laser wavelength with a wavelength meter having an accuracy of 600 MHz (HighFinesse WS-6). The laser passes through an optical isolator and is then coupled into a single mode fiber and sent to the atomic sample.

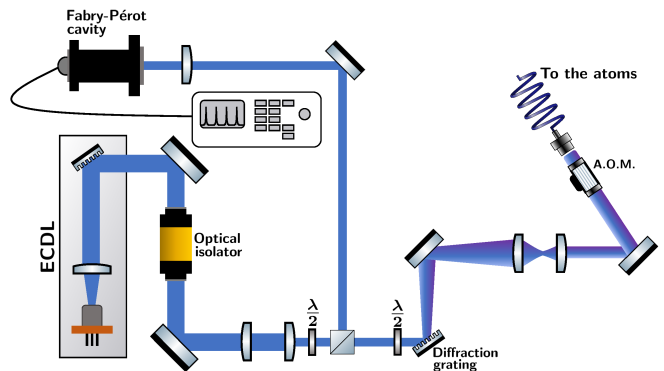


FIG. 3. Sketch of the experimental setup for the extended-cavity diode laser. The second diffraction grating, in combination with the single mode optical fiber, filters out most of the amplified spontaneous emission of the laser.

We observed that the lifetime of the trapped atoms was significantly affected by the blue laser even when operating at a power and detuning that should have small effect in a one-second timescale, see Fig. 4. We attribute this effect to the presence of a spectrally-broad background of amplified spontaneous emission (ASE), a fraction of which is in resonance with the atoms. Therefore we modified our setup to further clean the laser spectrum, see Fig. 3. The laser beam impinges onto another holographic grating, whose first diffraction order is injected into the fiber, so that the frequency spectrum gets filtered. To make a direct comparison we can inject the zero diffraction order of the grating into the fiber. Using the first diffraction order, the effect of the resonant light on the trapped atom lifetime is suppressed, see Fig. 4. We will discuss in detail the lifetime in the next section. Alternatively, we do not use the second grating but a tilted filter (Semrock LL01-405) that at the right angle cuts the low frequencies, including the light on resonance

with the atoms, up to six orders of magnitude.

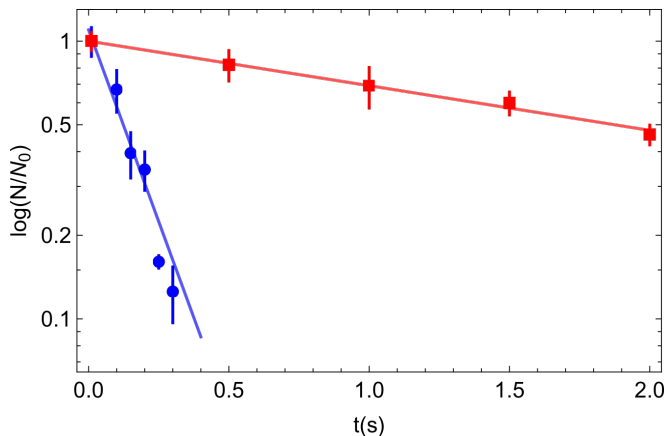


FIG. 4. Measured lifetime of a dysprosium Bose-Einstein condensate irradiated by the blue light. The lifetime with additional spectral filtering after the extended cavity (red dots) is (2.5 ± 0.3) s, much longer than the one without (blue dots), which is (120 ± 30) ms. Lines are exponential fits. The laser beam was Gaussian, with an average waist of $48 \mu\text{m}$ (see text), a power of 2 mW, and a wavelength of 403.6 nm.

2. Atomic system

The polarizability measurements are done on a Bose-Einstein condensate (BEC) of ^{162}Dy atoms. A beam of Dy atoms is slowed and cooled by a Zeeman slower and a laser operating on the 421 nm transition line. The atoms are then collected in a magneto-optical trap (MOT) operating on the 626 nm line, transferred to an infrared (IR) optical dipole trap enhanced by an in-vacuum cavity and finally trapped in two crossed IR beams where the final evaporation stage to condensation is realized. More details of the setup can be found in [23].

The light near 405 nm, coming from the fiber, passes through a quarter and a half waveplate in series to have a pure linear polarization, and is reflected by a polarizing beam splitter. Then it passes through another half waveplate and is reflected by a mirror and focused on the atoms by a 200 mm lens on the horizontal plane. The second half waveplate sets the angle between the laser polarization and the magnetization of the atoms, which is vertical. The final mirror has the two tilting screws regulated by two step motors; we calibrated the tilting angle on both axes as a function of the pulse duration given to the step motors. The laser power P is measured by two different calibrated power meter heads to minimize errors.

IV. MEASUREMENTS AND DISCUSSION

1. Measurement techniques

Our measurement technique relies on the momentum imparted to the atomic cloud by a pulse of repulsive light, as sketched in Fig. 5. The pulse duration δt is set by an acousto-optic modulator and a shutter before the fiber. After the light pulse we let the atoms expand freely and we detect them after a time of flight t_{exp} by absorption imaging along the vertical axis.

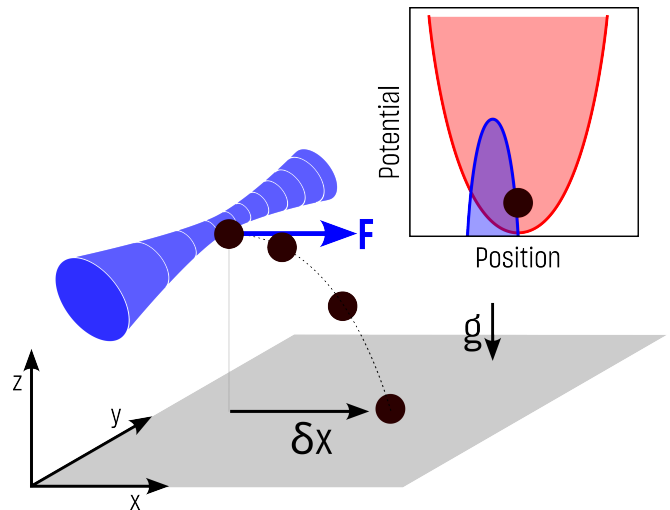


FIG. 5. Sketch of the method used to measure the polarizability. The repulsive blue beam is switched on for a small time δt and imparts a kick to the atoms while they are confined in the attractive infrared trap. In the subsequent expansion in the absence of optical trapping, the momentum kick translates into a displacement δx of the atomic center of mass in the horizontal plane xy , which is proportional to the dynamical polarizability. The x -axis is chosen to be the direction of the atomic displacement.

If we consider a Gaussian light beam propagating along y with waists w_x and w_z , and assume that the BEC is point-like, the atomic cloud will be subjected to a force in the direction x perpendicular to the propagation one [24],

$$F(x, z, \omega) = -\frac{dU(x, z, \omega)}{dx} = \frac{\text{Re}[\alpha(\omega)]}{2\epsilon_0 c} \frac{dI(x, z)}{dx}, \quad (7)$$

with $I(x, z) = I_0 e^{-2x^2/w_x^2} e^{-2z^2/w_z^2}$, where I_0 is the maximum laser intensity. Immediately after the pulse, we let the system expand for a time t_{exp} switching off the optical trapping and we measure the displacement δx of the cloud along in the horizontal plane. The displacement is proportional to the force as $\delta x = (F t_{exp} \delta t)/m$. The force, hence δx , has a dispersive behaviour as a function of the beam position with a maximum at $x = w_x/2$ and $z = 0$:

$$F_{max}(\omega) = \frac{2\sqrt{e} \text{Re}[\alpha(\omega)] P}{\pi \epsilon_0 c w_z w_x^2}, \quad (8)$$

where P is the laser power. If we take into account the finite dimensions of the BEC and we average over a Thomas-Fermi distribution calculated for 20×10^3 atoms in our IR harmonic trap, the maximum force decreases by 7%. Measuring δx for different beam positions in the xz plane allows us to derive the waist, as shown in Fig. 6, directly at the atom position, thus minimizing sources of errors typical in non-local measurements. Moreover, our measurement has a cubic dependence on the waist, while a measurement by the trap frequencies depends on the fourth power of the waist. Moving the beam along the horizontal axis, Fig. 6(a), we see that the displacement on the horizontal plane changes sign when we cross the atoms position. The measured δx has the shape of the spatial derivative of the beam intensity. Instead, along the vertical direction, Fig. 6(b), we observe on the horizontal plane just the intensity profile, i.e. a simple Gaussian shape. The fitted values of the waists are $w_x = (58 \pm 7) \mu\text{m}$, $w_z = (38 \pm 3) \mu\text{m}$, where the errors come from both the fitting errors and the calibration uncertainties.

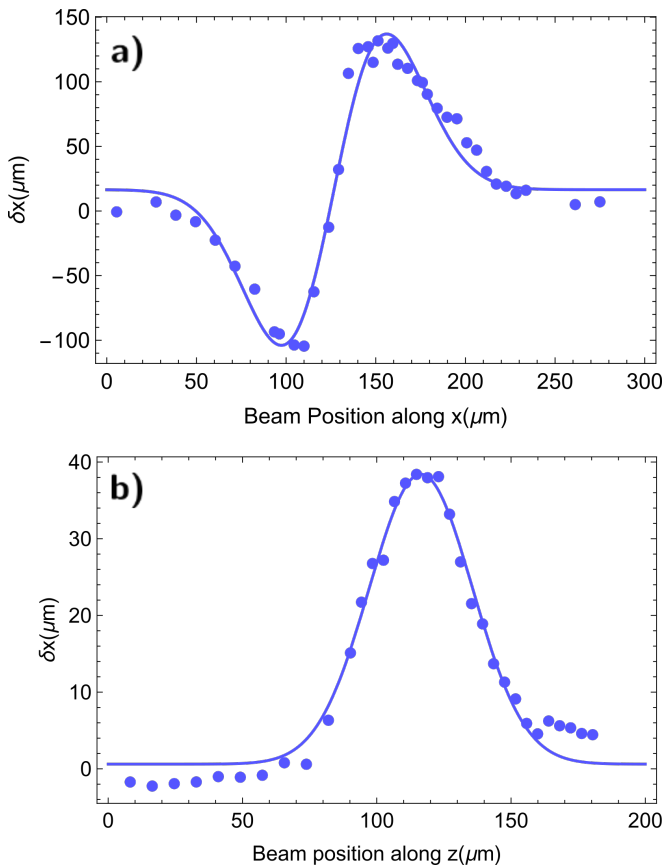


FIG. 6. Displacement measurements vs beam position. Displacement of the atomic center-of-mass δx on the horizontal plane as a function of the light beam position on the x -axis (a) and the z -axis (b).

The atoms undergo a maximum displacement δx_{max} ,

$$\delta x_{max}(\omega) = \frac{F_{max} t_{exp} \delta t}{m} = \frac{2\sqrt{e} \text{Re}[\alpha(\omega)] P t_{exp} \delta t}{\pi \epsilon_0 m c w_z w_x^2}. \quad (9)$$

Fixing the beam position to have $\delta x = \delta x_{max}$, a first measurement of the maximum displacement is done as a function of the polarization angle with respect to the magnetization, to find the relative contribution of the scalar and tensorial polarizabilities. The results of this are shown in Fig. 7(a), together with a fit done using Eq. 3.

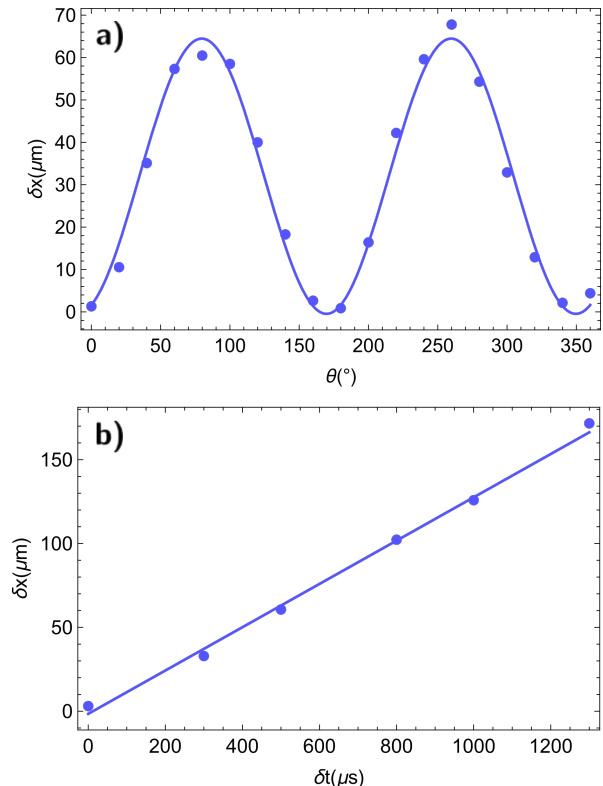


FIG. 7. Measurement of the scalar and tensorial polarizabilities: (a) Displacement δx of the atomic center-of-mass as a function of the angle θ of the light polarization with respect to the magnetization axis, together with the sinusoidal fit by Eq. 3 (line). (b) Displacement δx of the atomic center-of-mass as a function of the laser pulse duration δt together with a linear fit (line).

The fit parameters give the relative contributions of the scalar and tensorial polarizabilities. At this point we fix the half waveplate at the angle for which the atomic displacement is maximum, that is when the light polarization is perpendicular to the atomic magnetization, and we instead change the laser power or the laser pulse duration. Doing this we obtain a curve like that in Fig. 7b, if we remain in a regime where the displacement is linear. From the linear fit coefficient we can derive the absolute polarizability, inverting Eq. 9.

2. Experimental polarizability

We have repeated the polarizability measurements for a few wavelengths on the blue side of the 404.7 nm line. The measurements are shown in Fig. 8, together with the theoretical predictions from Eq.4. Also, the maximum polarizability is shown, occurring when the light polarization is perpendicular to the atomic magnetization. Considering the error bars, mainly due to the waist measurement, both the scalar and tensorial polarizabilities are in good agreement with the theoretical expectations. We did not extend the study closer to resonance, as the lifetime due to photon scattering becomes more critical. The real part of the polarizability scales with detuning Δ as Δ^{-1} , while the photon scattering rate, proportional to the imaginary part of the polarizability, as Δ^{-2} [18].

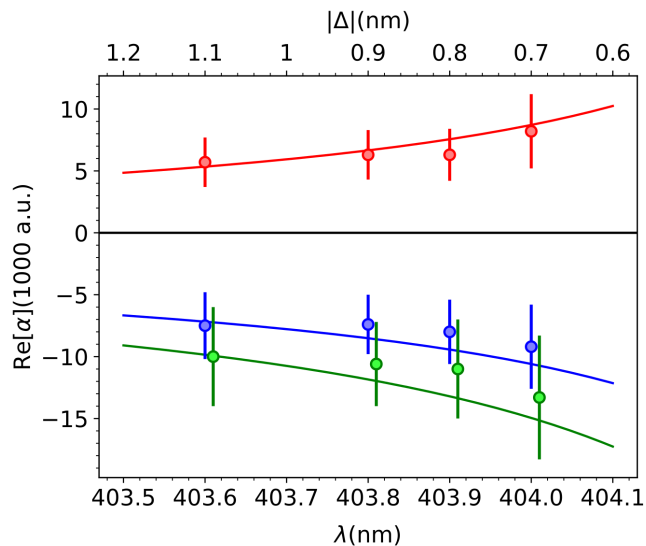


FIG. 8. Experimental polarizabilities as a function of the wavelength λ vs theoretical predictions. Scalar polarizability α_s (blue dots), tensorial polarizability α_t (red dots) and maximum polarizability $\alpha_s - \alpha_t/2$ (green dots) show a good agreement with the theoretical predictions (lines). The green dots are shifted by 0.01 nm to the right for clarity. The upper horizontal axis indicates the detuning Δ from the transition at 404.7 nm

3. Lifetime measurements

Concerning the lifetime of the BEC in presence of the blue light, the interpretation of what we observe in Fig. 4 must take into account the repulsive effect of the optical potential. In the condition of Fig. 4, i.e. laser power equal to 2 mW and wavelength of 403.6 nm, we expect a polarizability of about -10000 a.u. and a lifetime of about 400 ms if the atoms stay in the high intensity

region of the blue laser. However, the repulsive potential tends to expel the atoms from the high intensity region, leading to a new equilibrium position inside the combined IR and blue traps, where the intensity of the blue laser is lower. We did a modelization of the combined traps, and found that the equilibrium position moves by about one waist along x , meaning that the atoms feel a blue intensity reduced by a factor e^{-2} . Correspondingly, the lifetime increases by e^2 , which means up to 3 s, of the same order of magnitude of the experimental value, 2.5 s. We note that this value is of the same order of the lifetime of the BEC in the infrared trap alone. At the current stage, a precise measurement of the effect of the blue light on the lifetime is therefore not possible. Further experiments in which the repulsive potential gives a dominant and well-controlled contribution to the shape of the optical trap, for example in a box-like configuration, are required.

V. CONCLUSIONS

In conclusion, we reported the realization of a repulsive dipole potential for dysprosium atoms using a blue laser. We measured the scalar and tensorial polarizabilities near the 404.7 nm line, finding a good agreement with the theory. We observe a very large value of about -13000 a.u. for the maximum polarizability at 404 nm. This means that we can realize a repulsive potential of depth $U = k_B \times 500$ nK with just 1 mW of blue light on a Gaussian beam with a relatively large waist of 60 μ m. The lifetimes are of the order of 1 s, and are improved by the fact that the atoms do not stay in the highest intensity regions. We plan to employ this type of potential in future experiments on dipolar quantum gases. Particularly appealing is the possibility to realize a repulsive potential with a ring geometry for both superfluids and supersolids, to test the predicted differences in the rotation dynamics [17]. Furthermore, due to the strong tensor polarizability, light in the wavelength range explored in this work could be used to create controllable spin dependent potentials for dipolar atoms in different Zeeman states [25], which is extremely useful for the study of dipolar spin mixtures in optical lattices.

ACKNOWLEDGMENTS

Funded by the European Union (ERC, SUPER-SOLIDS, n.101055319) and by the QuantERA Programme, project MAQS, under Grant Agreement n.101017733, with funding organisation Consiglio Nazionale delle Ricerche. We acknowledge support from the European Union - NextGenerationEU for the “Integrated Infrastructure initiative in Photonics and Quantum Sciences” - I-PHOQS [IR0000016, ID D2B8D520, CUP B53C22001750006] and for the PNRR

-
- [1] A. L. Gaunt, T. F. Schmidutz, I. Gotlibovych, R. P. Smith, and Z. Hadzibabic, Bose-Einstein condensation of atoms in a uniform potential, *Phys. Rev. Lett.* **110**, 200406 (2013).
- [2] B. Mukherjee, Z. Yan, P. B. Patel, Z. Hadzibabic, T. Yefsah, J. Struck, and M. W. Zwierlein, Homogeneous atomic Fermi gases, *Phys. Rev. Lett.* **118**, 123401 (2017).
- [3] S. Krinner, D. Stadler, D. Husmann, J.-P. Brantut, and T. Esslinger, Observation of quantized conductance in neutral matter, *Nature* **517**, 64 (2015).
- [4] J. Billy, V. Josse, Z. Zuo, A. Bernard, B. Hambrecht, P. Lugan, D. Clément, L. Sanchez-Palencia, P. Bouyer, and A. Aspect, Direct observation of Anderson localization of matter waves in a controlled disorder, *Nature* **453**, 891 (2008).
- [5] W. J. Kwon, G. Del Pace, K. Khani, L. Galantucci, A. Muzi Falconi, M. Inguscio, F. Scazza, and G. Roati, Sound emission and annihilations in a programmable quantum vortex collider, *Nature* **600**, 64 (2021).
- [6] H. Kadau, M. Schmitt, M. Wenzel, C. Wink, T. Maier, I. Ferrier-Barbut, and T. Pfau, Observing the Rosensweig instability of a quantum ferrofluid, *Nature* **530**, 194 (2016).
- [7] L. Tanzi, E. Lucioni, F. Famà, J. Catani, A. Fioretti, C. Gabbanini, R. N. Bisset, L. Santos, and G. Modugno, Observation of a dipolar quantum gas with metastable supersolid properties, *Phys. Rev. Lett.* **122**, 130405 (2019).
- [8] F. Böttcher, J.-N. Schmidt, M. Wenzel, J. Hertkorn, M. Guo, T. Langen, and T. Pfau, Transient supersolid properties in an array of dipolar quantum droplets, *Phys. Rev. X* **9**, 011051 (2019).
- [9] L. Chomaz, D. Petter, P. Ilzhöfer, G. Natale, A. Trautmann, C. Politi, G. Durastante, R. M. W. van Bijnen, A. Patscheider, M. Sohmen, M. J. Mark, and F. Ferlaino, Long-lived and transient supersolid behaviors in dipolar quantum gases, *Phys. Rev. X* **9**, 021012 (2019).
- [10] L. Su, A. Douglas, M. Szurek, R. Groth, S. F. Ozturk, A. Krahn, A. H. Hébert, G. A. Phelps, S. Ebadi, S. Dickerson, F. Ferlaino, O. Marković, and M. Greiner, Dipolar quantum solids emerging in a Hubbard quantum simulator, *Nature* **622**, 724–729 (2023).
- [11] C. Ravensbergen, V. Corre, E. Soave, M. Kreyer, S. Tzanova, E. Kirilov, and R. Grimm, Accurate determination of the dynamical polarizability of dysprosium, *Physical review letters* **120**, 223001 (2018).
- [12] M. Kreyer, J. H. Han, C. Ravensbergen, V. Corre, E. Soave, E. Kirilov, and R. Grimm, Measurement of the dynamic polarizability of Dy atoms near the 626-nm intercombination line, *Physical Review A* **104**, 033106 (2021).
- [13] T. Chalopin, V. Makhlov, C. Bouazza, A. Evrard, A. Barker, M. Lepers, J.-F. Wyart, O. Dulieu, J. Dalibard, R. Lopes, *et al.*, Anisotropic light shift and magic polarization of the intercombination line of dysprosium atoms in a far-detuned dipole trap, *Physical Review A* **98**, 040502 (2018).
- [14] J. H. Becher, S. Baier, K. Aikawa, M. Lepers, J.-F. Wyart, O. Dulieu, and F. Ferlaino, Anisotropic polarizability of erbium atoms, *Physical Review A* **97**, 012509 (2018).
- [15] V. Dzuba, V. Flambaum, and B. L. Lev, Dynamic polarizabilities and magic wavelengths for dysprosium, *Physical Review A* **83**, 032502 (2011).
- [16] H. Li, J.-F. Wyart, O. Dulieu, S. Nascimbene, and M. Lepers, Optical trapping of ultracold dysprosium atoms: transition probabilities, dynamic dipole polarizabilities and van der Waals C6 coefficients, *Journal of Physics B: Atomic, Molecular and Optical Physics* **50**, 014005 (2016).
- [17] A. J. Leggett, Can a solid be “superfluid”?, *Phys. Rev. Lett.* **25**, 1543 (1970).
- [18] R. Grimm, M. Weidemüller, and Y. Ovchinnikov, Optical dipole traps for neutral atoms, *Advances in Atomic Molecular and Optical Physics* **42**, 95 (2000).
- [19] M. Kreyer, J. Han, C. Ravensbergen, V. Corre, E. Soave, E. Kirilov, and R. Grimm, Measurement of the dynamic polarizability of Dy atoms near the 626-nm intercombination line, *Phys.Rev.A* **104**, 033106 (2021).
- [20] J. Mitroy, M. Safronova, and C. Clark, Theory and applications of atomic and ionic polarizabilities, *Journal of Physics B: Atomic, Molecular and Optical Physics* **43**, 202001 (2010).
- [21] M. Wickliffe, J. Lawler, and G. Nave, Atomic transition probabilities for Dy I and Dy II, *JQRST* **66**, 363 (2000).
- [22] J. E. Sansonetti and W. C. Martin, Handbook of basic atomic spectroscopic data, *Journal of physical and chemical reference data* **34**, 1559 (2005).
- [23] E. Lucioni, L. Tanzi, A. Fregosi, J. Catani, S. Gozzini, M. Inguscio, A. Fioretti, C. Gabbanini, and G. Modugno, Dysprosium dipolar Bose-Einstein condensate with broad Feshbach resonances, *Phys. Rev. A* **97**, 060701(R) (2018).
- [24] A force along the z direction is also applied, given by $-dU/dz$. However, we do not measure this component of the force because with our imaging we integrate in the z direction and we observe only the xy plane.
- [25] L. Du, P. Barral, M. Cantara, J. de Hond, Y. Lu, and W. Ketterle, Atomic physics on a 50 nm scale: Realization of a bilayer system of dipolar atoms, [arXiv:physics/9902072v1](https://arxiv.org/abs/physics/9902072v1) (2023).